

Phase Frustration-Induced Spatial Lattice Symmetry in the Vicsek-Kuramoto-Sakaguchi Model

Yichen Lu

September 4, 2025

Contents

1	The Model	1
2	Phase Frustration-Induced Crystallization	3
2.1	Key properties	3
2.1.1	Snapshots and phase diagram	4
2.1.2	Respiration-like motion of unit cells	6
2.1.3	Initial conditions determined cells composition	8
3	Critical condition for phase transition and mechanism	9
3.1	Linear stability analysis with amplitude ansatz	9

1 The Model

Particles have a spatial position $\mathbf{r}_i = (x_i, y_i)$ and an internal phase θ_i which evolve according to equations:

$$\dot{\mathbf{r}}_i = v \mathbf{p}(\theta_i) , \quad (1a)$$

$$\dot{\theta}_i = \frac{K}{|A_i|} \sum_{j \in A_i} [\sin(\theta_j - \theta_i + \alpha) - \sin \alpha] , \quad (1b)$$

for $i = 1, 2, \dots, N$. Here in Eq. (1a), $\mathbf{p}(\theta) = (\cos \theta, \sin \theta)$, which means each particle rotates with a constant speed v in the direction of its instantaneous phase $\theta_i(t)$. The particles are treated as point-like with no direct spatial interactions, consistent with classical models of chiral self-propelled particles [1–3, 7, 8]. As per Eq. (1b), the mean runs over neighbors within a coupling radius d_0 around particle i :

$$A_i(t) = \{j \mid |\mathbf{r}_i(t) - \mathbf{r}_j(t)| \leq d_0\} , \quad (2)$$

$K (\geq 0)$ is the coupling strength, α is the phase frustration between two neighboring particles. When $\alpha_0 = 0$, the dynamics reduces to the normal Vicsek-like model. The introduction of counter term $-\sin \alpha$ ensures that the interaction force cancels exactly when phase differences vanish ($\theta_j - \theta_i = 0$). This guarantees that perfect synchronization is always an equilibrium state. Without this term, synchronized oscillators would experience a net force $K \sin \alpha$, artificially shifting their frequencies [6].

Some necessary order parameters can be introduced to measure the level of coordination among swarmalators in space motion and phase dynamics. Firstly, at the macroscopic level, the system may be described by the single-partial distribution $\rho(\mathbf{r}, \theta, t)$, which satisfies the normalization condition

$$\int_{L \times L} d^2 \mathbf{r} \int_0^{2\pi} d\theta \rho(\mathbf{r}, \theta, t) = 1 , \quad (3)$$

where L is the size of the system in two dimensions. Next, we define the coarse-grained spatial density $\varrho(\mathbf{r}, t)$ and the global polarization $p(\theta, t)$ density by integrating $\rho(\mathbf{r}, \theta, t)$ over the phase and spatial, respectively:

$$\varrho(\mathbf{r}, t) = \int_0^{2\pi} \rho(\mathbf{r}, \theta, t) d\theta , \quad (4a)$$

$$p(\theta, t) = \int_{L \times L} \rho(\mathbf{r}, \theta, t) d\mathbf{r} . \quad (4b)$$

In the homogeneous state, these quantities take uniform values $(\rho, \varrho, p) = (\rho_0, \varrho_0, p_0) = (1/(2\pi L^2), 1/L^2, 1/2\pi)$.

To measure deviations from uniformity, we define the following single-particle order parameters:

$$\rho_{\text{std}}(t) = \frac{1}{1 - \rho_0} \left[\max_{\mathbf{r} \in L \times L, \theta \in [0, 2\pi]} \rho(\mathbf{r}, \theta, t) - \rho_0 \right] , \quad (5)$$

Similarly, we can define order parameters for spatial and phase polarization densities, denoted as ϱ_{std} and p_{std} , respectively. These order parameters range from 0 to 1, reflecting the degree of spatial and phase coherence in the system. When particles are uniformly distributed in both space and phase, $\rho, \varrho, p_{\text{std}} \approx 0$. Conversely, if full condensation and polarization occur, $\rho, \varrho, p_{\text{std}} \approx 1$.

We conducted numerical simulations to investigate the performance and characteristics of our system under various conditions. For simplicity, we assume that particles are initially distributed uniformly in a two-dimensional $L \times L$ square with periodic boundary conditions. Unless otherwise stated, all the numerical simulations of the model Eq. (1) were run on Python using Euler integration with box size of $L = 7$, population sizes of $N = 2000$, self-propulsion speed of $v = 3$. For the final state and phase diagram, each data point of order parameters was collected by averaging last 500 time steps of the simulation to discard the transients.

2 Phase Frustration-Induced Crystallization

2.1 Key properties

1. [Done] What does the lattice structure look like? What is the unit cell structure, and what is the spatial arrangement of the unit cells? Besides triangular, what other spatial structures exist? In which regions of frustration does it appear? (And what are the corresponding coupling conditions and natural frequency distributions?)

Lattice structure emerges when $\alpha \in (\pi/2, \pi]$. For $\pi/2 < \alpha \ll \pi$, the lattice structure exhibits a triangular arrangement (Sometimes it is a tetragonal lattice, but in most cases it is stable in a triangular lattice), where in each cell, particles are arranged in a vortex pattern independent of natural frequency (mainly determined by initial conditions). This arrangement leads to a stable and ordered configuration, where the cells maintain a fixed distance from each other and the particles rotate in a coordinated manner in the form of cycloids, which leads to respiration-like motion of the cells. While for $\alpha = \pi$ (anti-alignment coupling), the system transforms into a double-lane structure with particles in each lane propelling in opposite directions.

2. [Done] What is each cell composed of?

Each cell is composed of particles with the neighboring particles at initial conditions, whose criterion is discussed in Sec. 2.1.3.

3. [Done] What is the internal dynamics within a cell?

Within a cell, particles are all-to-all coupled, and they rotate in a Kuramoto-like manner.

4. [Done] What determines the length (periodicity)? (Interaction distance?)

The lattice constant (distance) is determined by the coupling strength K , the radius d_0 , and the frustration α . For $\alpha \gtrsim 0.5\pi$ The theoretical lattice constant is given by Eq. (7).

2.1.1 Snapshots and phase diagram

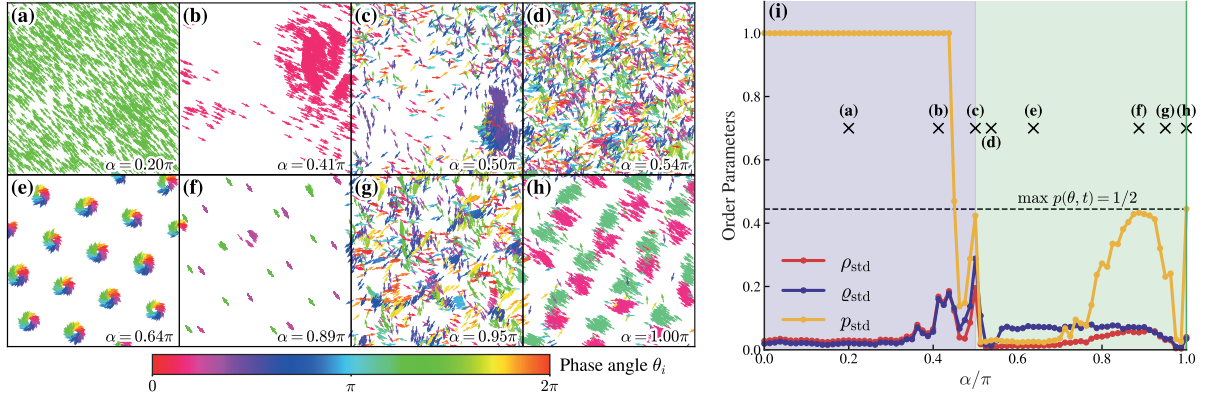


Figure 1: (a)-(h) Representative simulation snapshots for synchronization state [(a)-(c)] and lattice state [(d)-(h)] at different phase frustration α . (i) Phase diagram and order parameters of the system with respect to the phase frustration α . The crosses mark the snapshots in (a)-(h). Regions of blue and green respectively represent the synchronization and lattice states. The horizontal dashed line indicates the values of the value of order parameter p_{std} when $\max p(\theta, t) = 1/2$ (Dual cluster synchronization). Parameters: $K = 20$, $d_0 = 1.55$, $L = 7$.

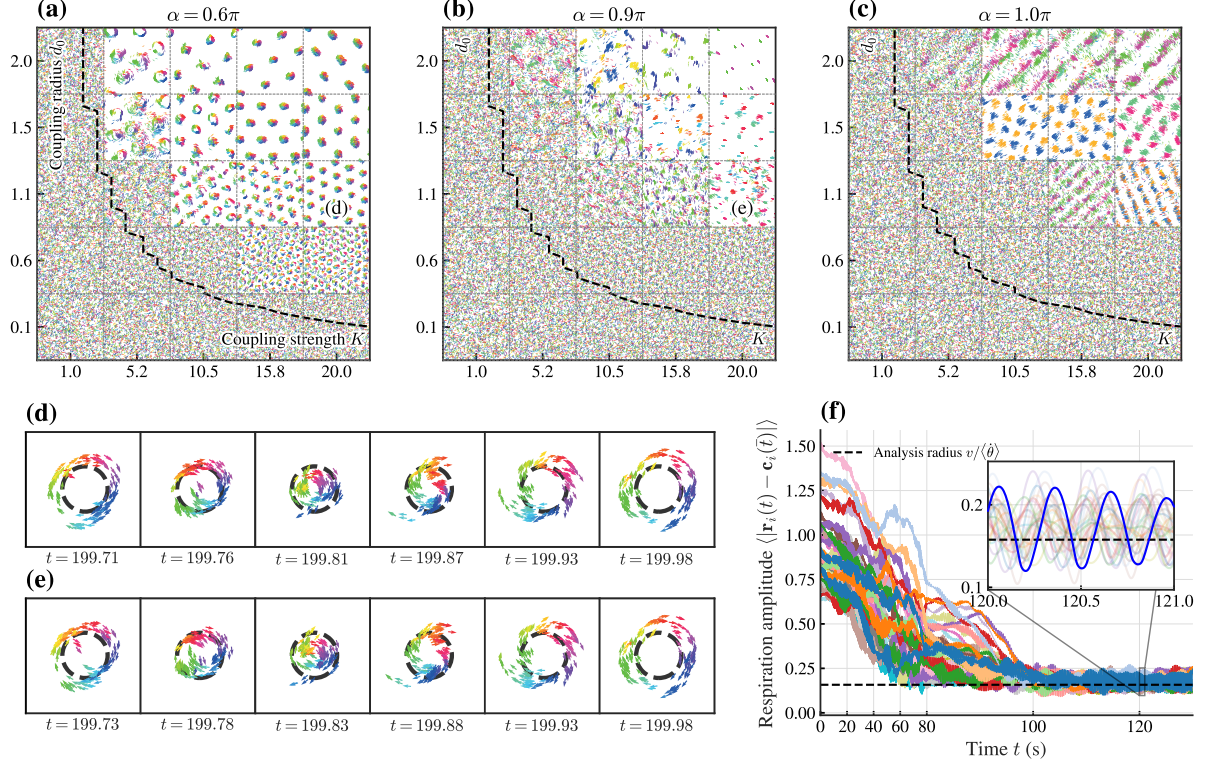


Figure 2: (a)-(c) Snapshots of (K, d_0) phase diagram for different frustration α at system size $L = 7$. The regions of manifest and cryptic lattice states are indicated by the black dashed lines given by Eq. (19). (d)

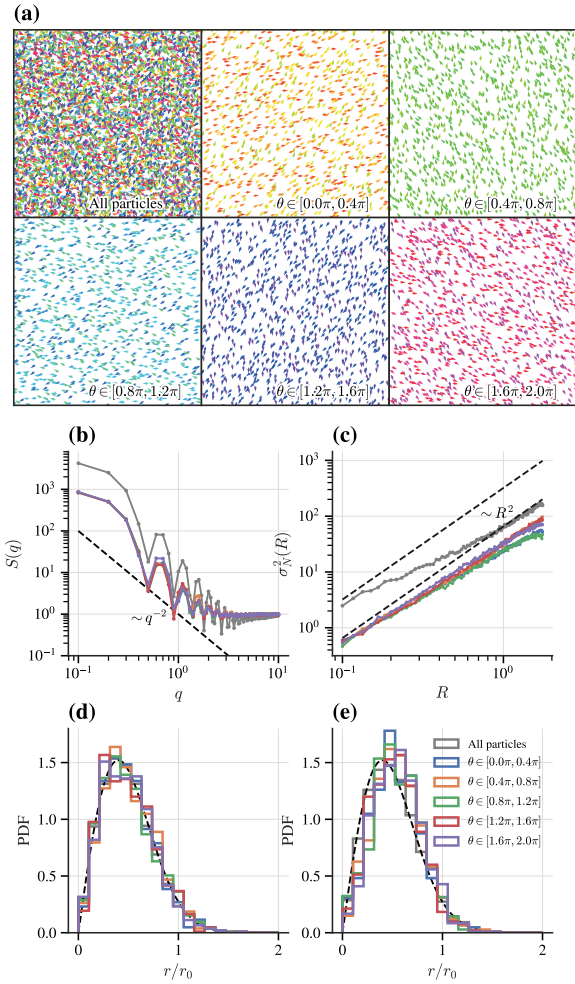


Figure 3: 1

2.1.2 Respiration-like motion of unit cells

For $\alpha = 0.6\pi$, the system exhibits the respiration-like motion of the cells. Since the phases of particles in each cell are uniformly distributed in $[0, 2\pi]$ and the distance between cells is large enough to be considered decoupled, the effective frequency of each particle can be approximated by

$$\dot{\theta}_i = -K \sin \alpha + \frac{K}{|A_i|} \int_0^{2\pi} d\theta' \sin(\theta' - \theta_i + \alpha) = -K \sin \alpha , \quad (6)$$

and the lattice constant a can be approximated as

$$a = d_0 + 2 \frac{v}{K |\sin \alpha|} . \quad (7)$$

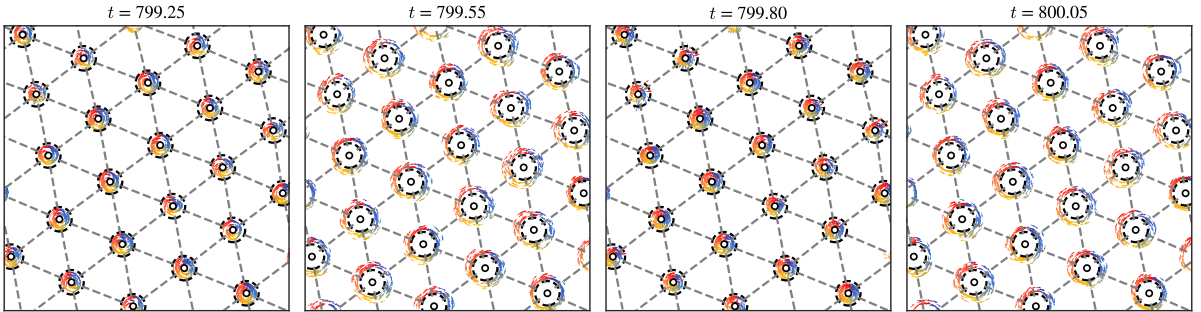


Figure 4: respiration-like motion of the cells with $\omega_{\min} = 0$, $\Delta\omega = 0$, $N = 3000$, $K = 10.5$, $d_0 = 1.07$, and $\alpha = 0.6\pi$. Black hollow dots represent the center of mass of each cell, black dash circles represent the theoretical unit cell radius $v/\dot{\theta}_i$, and the gray dash lines represent the theoretical distance between unit cells d_0 .

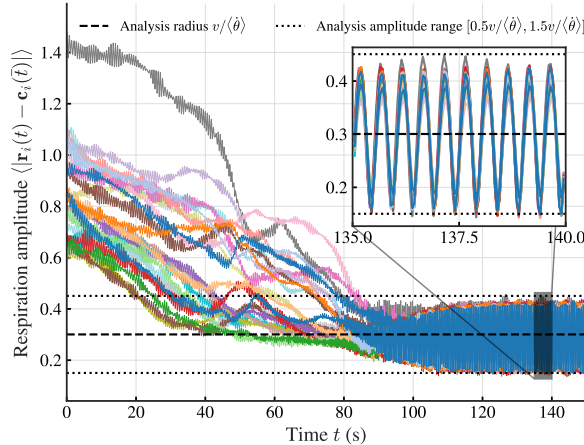


Figure 5: respiration amplitude of the system. The parameters are the same as in Fig. 4. Different colors represent different cells, and the amplitude is defined as the distance between particles and the center of mass of the cell at final state ($\bar{t} = 40$).

As shown in Fig. 4 and Fig. 5, the respiration amplitude of the cells is defined as $\langle |\mathbf{r}_i(t) - \mathbf{c}_i(\bar{t})| \rangle$, where $\mathbf{c}_i(\bar{t})$ is the center of mass of the cell of i -th particle at final state ($\bar{t} = 40$), and $\langle \cdot \rangle$ denotes the average over all particles in the cell. It is worth noting that the amplitude is fluctuating around the theoretical cell radius $v/\dot{\theta}_i$ and the respiration frequency of the cells exhibit synchronization.

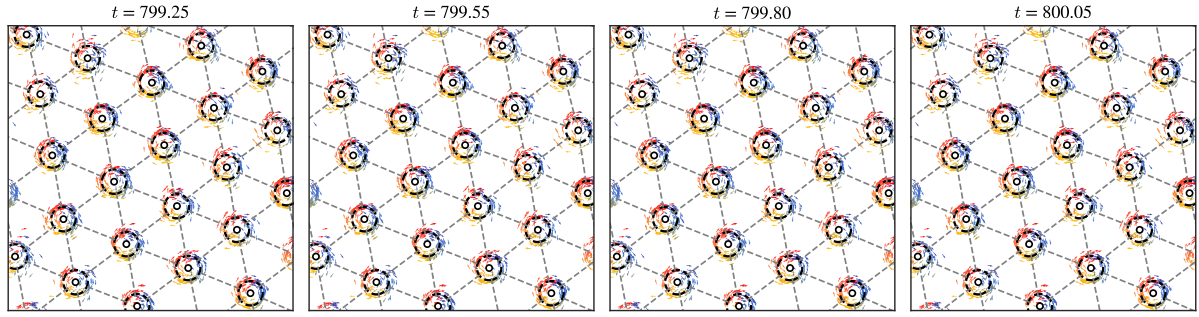


Figure 6: respiration-like motion of the decoupled cells. The parameters are the same as in Fig. 4.

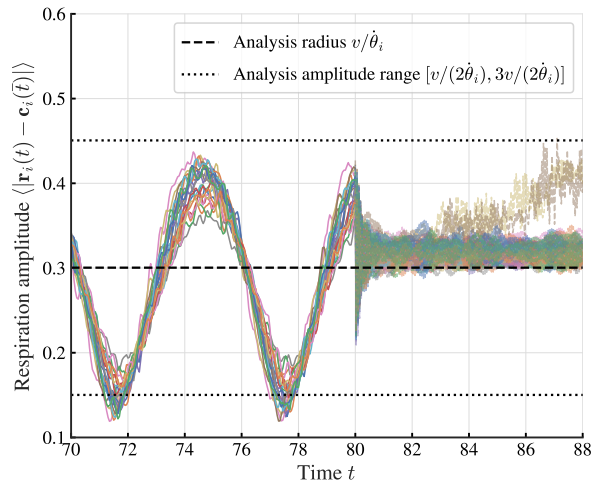


Figure 7: Respiration amplitude of the decoupled cells ($t > 80$). The parameters are the same as in Fig. 4.

2.1.3 Initial conditions determined cells composition

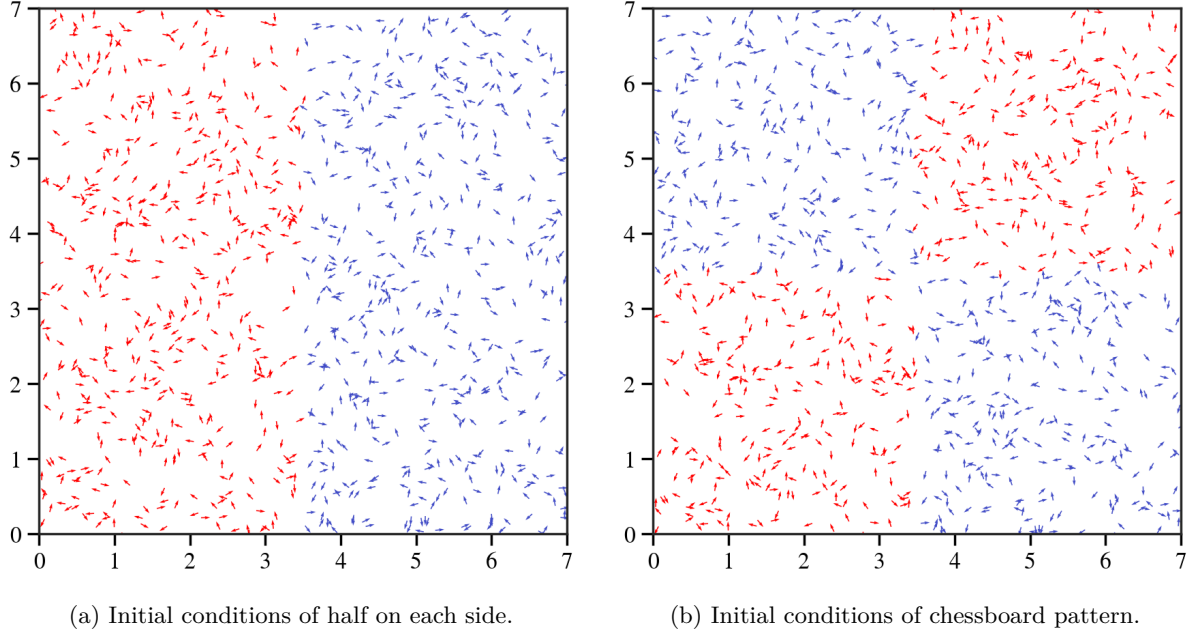


Figure 8: Two artificial non-uniform initial conditions in space. Red and blue particles represent particles with positive and negative chirality, respectively.

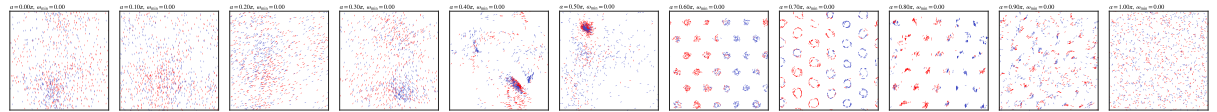


Figure 9: Snapshot of the system at $t = 80$ with $N = 1000$, $K = 20$, $\omega_{\min} = 0$, $\Delta\omega = 1$ and initial conditions of half on each side.

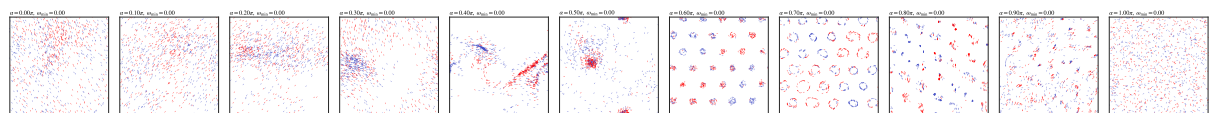


Figure 10: Snapshot of the system at $t = 80$ with $N = 1000$, $K = 20$, $\omega_{\min} = 0$, $\Delta\omega = 1$ and initial conditions of chessboard pattern.

3 Critical condition for phase transition and mechanism

3.1 Linear stability analysis with amplitude ansatz

In the thermodynamic limit $N \rightarrow \infty$, the state of the system in Eq. (1) can be characterized by the single-partial distribution $\rho(\mathbf{r}, \theta, t)$, which satisfies the continuity equation

$$\frac{\partial \rho}{\partial t} = -v \mathbf{p}(\theta) \cdot \nabla \rho - \frac{\partial}{\partial \theta} \{ \mathcal{T}[\rho] \rho \} , \quad (8)$$

where \mathcal{T} is the linear operator that has the form

$$\begin{aligned} \mathcal{T}[\rho] = & \frac{K}{A} \int_{L \times L} d^2 \mathbf{r}' \int_0^{2\pi} d\theta' \rho(\mathbf{r}', \theta', t) \\ & \times \Theta(d_0 - |\mathbf{r}' - \mathbf{r}|) [\sin(\theta' - \theta + \alpha) - \sin \alpha] , \end{aligned} \quad (9)$$

where $\Theta(r)$ is Heaviside step function and

$$A = \int_{L \times L} d^2 \mathbf{r}' \int_0^{2\pi} d\theta' \rho(\mathbf{r}', \theta', t) \Theta(d_0 - |\mathbf{r}' - \mathbf{r}|) . \quad (10)$$

One obvious solution of Eq. (8) is $\rho = (2\pi L^2)^{-1}$ representing a uniform disordered state. The stability of such a solution can be investigated by considering a small perturbation,

$$\rho(\mathbf{r}, \theta, t) = \frac{1}{2\pi L^2} + \varepsilon e^{\lambda(k)t+i\mathbf{k}\cdot\mathbf{r}} \Phi(\theta) , \quad (11)$$

with $k = |\mathbf{k}| > 0$, and linearizing the non-linear continuity equation (8), obtaining a eigenvalues problem to compute the $\lambda(k)$ spectrum

$$(\mathcal{L}_0 - ivk\mathcal{L}_1) \Phi = \lambda \Phi , \quad (12)$$

\mathcal{L}_0 is diagonal in the basis $\{e^{im\theta}\}_{m=-\infty}^{\infty}$,

$$\mathcal{L}_0 \Phi_m = \lambda_m^{[0]} e^{im\theta} , \quad (13)$$

with the eigenvalues

$$\lambda_m^{[0]}(k) = \frac{K J_1(kd_0)}{kd_0} (\delta_{m,-1} e^{i\alpha} + \delta_{m,1} e^{-i\alpha}) , \quad (14)$$

where $J_1(x)$ is the Bessel function of the first kind of order one. The operator \mathcal{L}_1 is defined as

$$\mathcal{L}_1 e^{im\theta} = \frac{1}{2} (e^{i(m+1)\theta-i\vartheta} + e^{i(m-1)\theta+i\vartheta}) , \quad (15)$$

where ϑ is the forms \mathbf{k} with the x axis. Without the loss of generality, we can define the x axis parallel to \mathbf{k} , and, therefore, take $\vartheta = 0$.

Therefore, we have the characteristic polynomial

$$P_{2M+1}(\lambda) = \begin{vmatrix} \lambda_{-M}^{[0]} - \lambda & b & \dots & 0 \\ b & \lambda_{-M+1}^{[0]} - \lambda & b & \vdots \\ \vdots & b & \ddots & b \\ 0 & \dots & b & \lambda_M^{[0]} - \lambda \end{vmatrix} , \quad (16)$$

where $b = -ikv/2$. For analytical convenience, we truncate the expansion at order $M = 2$, resulting in a polynomial of degree 5 with the following coefficients:

$$\begin{aligned} c_5 &= 1, \quad c_4 = -\frac{2KJ_1(d_0k)\cos\alpha}{d_0k}, \quad c_3 = \frac{K^2 J_1^2(d_0k)}{d_0^2 k^2} + k^2 v^2 \\ c_2 &= -\frac{Kkv^2 J_1(d_0k)\cos\alpha}{d_0}, \quad c_1 = \frac{3k^4 v^4}{16}, \quad c_0 = 0 . \end{aligned} \quad (17)$$

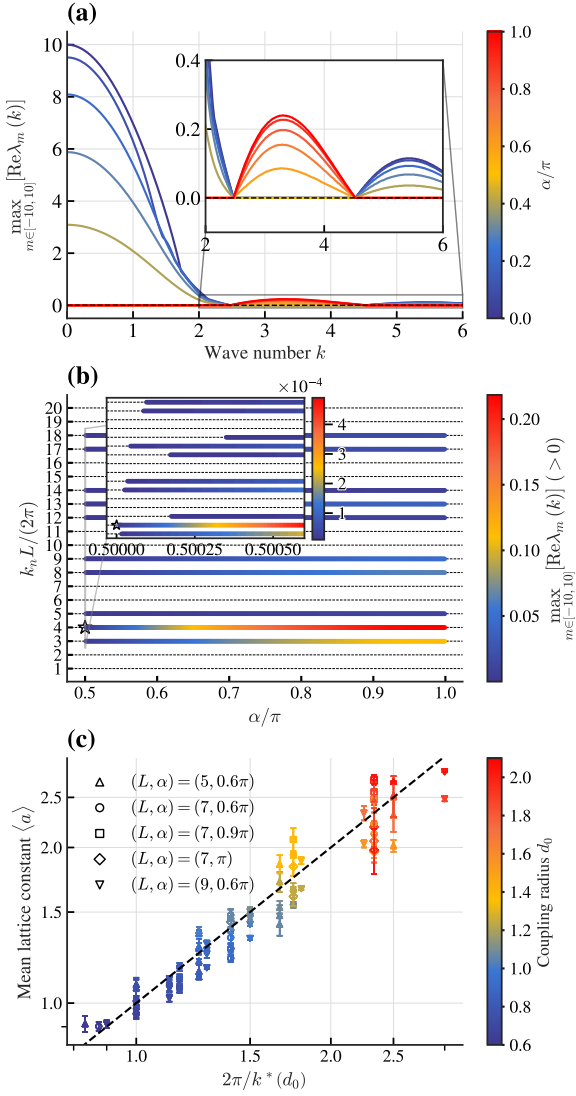


Figure 11: (a)-(b) Computations of the $\lambda(k)$ with the largest real part as a function of the continuous wavenumber k [(a)] and standardized discrete wavenumber $\bar{k}L/(2\pi)$ [(b)] and α in the truncated basis $M = 10$. Other parameters as in Fig. 1. Insets: magnified views. (b) Thick colored lines denote positive eigenvalues (unstable modes), while thin dashed lines indicate stable modes. Stars mark the first unstable wavenumber at criticality. (c) Measured mean lattice constant $\langle a \rangle$ compared to theoretical prediction. Horizontal and vertical error bars represent standard deviations across K and unit cells, respectively. The black dashed line indicates a 1:1 correspondence.

It is evident that $\lambda = 0$ is always a root of the characteristic polynomial. To analyze the signs of the remaining eigenvalues, we factor out this zero root and apply the Routh–Hurwitz criterion to the reduced polynomial. This yields a necessary and sufficient condition for system stability:

$$J_1(d_0 k) \cos \alpha < 0 , \quad (18)$$

This inequality shows that stability depends on the interplay among the frustration α (critical at $\pi/2$), coupling distance d_0 , and the wavenumber k , but is independent of the coupling strength K . This analytical conclusion aligns with the numerical results presented in Fig. 11(c), where the lattice constant remains unaffected by K in the manifest lattice states.

The periodic boundary conditions lead to quantization conditions on the wavenumber k , resulting in discrete wavenumbers $k_n = 2\pi n/L$.

$$\frac{2\pi}{k^*(d_0)} = \frac{2v}{K} \quad (19)$$

References

- [1] Michel Fruchart, Ryo Hanai, Peter B. Littlewood, and Vincenzo Vitelli. Non-reciprocal phase transitions. *Nature*, 592(7854):363–369, Apr 2021.
- [2] D. Levis, I. Pagonabarraga, and B. Liebchen. Activity induced synchronization: Mutual flocking and chiral self-sorting. *Phys. Rev. Res.*, 1:023026, Sep 2019.
- [3] Benno Liebchen and Demian Levis. Collective behavior of chiral active matter: Pattern formation and enhanced flocking. *Phys. Rev. Lett.*, 119:058002, Aug 2017.
- [4] Edward Ott and Thomas M. Antonsen. Low dimensional behavior of large systems of globally coupled oscillators. *Chaos: An Interdisciplinary Journal of Nonlinear Science*, 18(3):037113, 09 2008.
- [5] Edward Ott and Thomas M. Antonsen. Long time evolution of phase oscillator systems. *Chaos: An Interdisciplinary Journal of Nonlinear Science*, 19(2):023117, 05 2009.
- [6] Hidetsugu Sakaguchi, Shigeru Shinomoto, and Yoshiki Kuramoto. Mutual entrainment in oscillator lattices with nonvariational type interaction. *Progress of Theoretical Physics*, 79(5):1069–1079, 05 1988.
- [7] Bruno Ventejou, Hugues Chaté, Raul Montagne, and Xia-qing Shi. Susceptibility of orientationally ordered active matter to chirality disorder. *Phys. Rev. Lett.*, 127:238001, Nov 2021.
- [8] Yujia Wang, Bruno Ventéjou, Hugues Chaté, and Xia-qing Shi. Condensation and synchronization in aligning chiral active matter. *Phys. Rev. Lett.*, 133:258302, Dec 2024.